Supporting Information:

A Codeposition Route to CuI-Pyridine Coordination Complexes for OLEDs

Zhiwei Liu,[†] Munzarin F. Qayyum,[‡] Chao Wu,[†] Matthew T. Whited,[†] Peter I. Djurovich,[†] Keith O. Hodgson,[‡,§] Britt Hedman,[§] Edward I. Solomon,[‡] and Mark E. Thompson[†]*

[†]Department of Chemistry, University of Southern California, Los Angeles, California 90089, [‡]Department of Chemistry, Stanford University, Stanford, California 94305, and [§]Stanford Synchrotron Radiation Lightsource, SLAC, Stanford University, Stanford, California 94309

E-mail: met@usc.edu

General: All the starting chemicals were purchased from commercial resources and used as received. Solvents for preparing copper complexes were degassed prior to use. All reactions were performed under N_2 atmosphere. ^{1}H-NMR spectrum was recorded on a Varian-500MR NMR spectrometer. Chemical shift data for each signal were reported in ppm units with $CDCl_3$ as reference, where δ ($CDCl_3$) = 7.26. Elemental analyses were performed on a Model CE 440 CHN Analyzer.

Synthesis of mCPy: A mixture of carbazole (3.67 g, 22 mmol), 3, 5-dibromopyridine (2.37 g, 10 mmol), potassium carbonate (3.04 g, 22 mmol), copper powder (0.6 g) and nitrobenzene (30 mL) was heated to 220°C for overnight. The mixture was then distillated at reduced pressure. The obtained residue was extracted with dichloromethane and purified by column chromatography on silica gel with hexane/ dichloromethane. The product was further purified by double sublimation at low pressure (10^{-5} torr). Total yield: 46%. ^{1}H-NMR (500 MHZ, $CDCl_3$): δ 9.13 (br, 2H), 8.19 (s, 1H), 8.18 (d, J = 8.0 Hz, 4H), 7.54 (d, J = 8.5 Hz, 4H), 7.48 (t, J = 7.5 Hz, 4H), 7.36 (t, J = 7.5 Hz, 4H). Anal. Calcd. for $C_{29}H_{19}N_3$: C, 85.06; H, 4.68; N, 10.26. Found: C, 85.54; H, 4.52; N, 10.31. MS *m/z*: 409

Synthesis of [CuI(mCPy)]$_\infty$ (model A): This was synthesized via two methods. The first, the method reported for [CuI(py)]$_\infty$, involved the addition of CuI (116 mg, 0.61 mmol) and mCPy (247 mg, 0.60

mmol) to acetonitrile (150 mL) at 60°C to obtain a clear solution. After 2 days, $[CuI(py)]_\infty$ was obtained upon cooling. The second method involved the addition of mCPy (102 mg, 0.25 mmol) in dichloromethane (10 mL) to the solution of CuI (48 mg, 0.25 mmol) in acetonitrile (10 mL). The product, which precipitated immediately, washed with dichloromethane, acetonitrile and dried in vacuo. Anal. Calcd. for $C_{29}H_{19}CuIN_3$: C, 58.06; H, 3.19; N, 7.00. Found: C, 57.86; H, 2.84; N, 6.89.

Synthesis of $[CuI\ (mCPy)]_4 \cdot 3CH_2Cl_2$ (model B1): The crystals were obtained by addition of CuI (10 mg) in a small amount of acetonitrile to excess of mCPy in dichloromethane. White crystals with green emission were obtained overnight. The product was stored under dichloromethane saturated nitrogen. Exposing to air gave orange emission product, which can be transferred immediately back to the green form under dichloromethane vapor or in dichloromethane.

Preparation of $[CuI(mCPy)]_4$ (model B2): The model **B2** was obtained by treating **B1** in vacuo or exposing **B1** in air overnight. The model **B2** can also be converted back to **B1** in the presence of CH_2Cl_2 vapor.

Preparation of model D: 1.8 μm CuI:mCPy films (ratio = 1:2.5) were deposited on five four-inch Si wafers in vacuum chamber and scraped off to give about 40 mg powder sample (model **D**). The sample shows identical photophysical properties to the codeposited films, that is, a maximum emission band around 530 nm, and decay lifetimes of 2.5 (23%) and 7.7 (77%) μs at room temperature.

X-ray Crystallography: The crystal was mounted on a glass fiber with Paratone-N oil. X-ray diffraction data were collected on a Bruker SMART APEX diffractometer using graphite-monochromated Mo Kα radiation, and structures were determined using direct methods with standard Fourier techniques using the Bruker AXS software package.

Photophysical Measurements: Both photoluminescence and electroluminescence spectra were measured by a PTI QuantaMaster model C-60SE spectrophotometer, equipped with a 928 PMT detector and corrected for detector response. Phosphorescent lifetimes were measured by time-correlated single-photon counting using an IBH Fluorocube instrument equipped with a 331 nm LED excitation source.

Quantum yield measurements were carried out using a Hamamatsu C9920 system equipped with a xenon lamp, calibrated integrating sphere and model C10027 photonic multichannel analyzer.

OLEDs Fabrication and Testing: All devices were fabricated in a Kurt J. Lesker vacuum thermal evaporation chamber. Patterned ITO was cleaned with Alconox, acetone, AZ 1512 photoresist, and acetone followed by ultraviolet (UV) ozone treatment. After the deposition of organic layers, the substrates were taken out, a shadow mask was placed on and the substrates were then loaded into the chamber again to complete the cathode LiF (1 nm)/ Al (100 nm). The electrical and optical characteristics of the devices were measured with a Keithly 2400 source/meter/2000 multimeter coupled to a Newport 1835-C optical meter, equipped with a UV 818 Si photo detector in ambient atmosphere and at room temperature.

XAS Sample Preparation: Model **D** was ground in two-third by weight in boron nitride in order to reduce self-absorption. The powdered complex was then stirred into mineral oil to make a homogenous mull. ~150 μL of the mull sample was loaded into a 2 mm Delrin XAS cell with a 38 μm Kapton window and frozen immediately in a hexane/liquid nitrogen slush to prevent the solid particles in the mull from settling to the bottom. A similar sample was prepared by directly mixing model **D** in mineral oil without grinding. The two samples provided identical XAS data. The $[CuI(mCPy)]_\infty$ polymer sample (model **A**) was prepared following the latter procedure (without grinding).

XAS Data Acquisition: XAS data of the mull samples were measured at the Cu K-edge at Stanford Synchrotron Radiation Lightsource (SSRL) on the focused 16-pole, 2.0-T wiggler beam line 9-3 under storage ring parameters of 3 GeV and ~300 mA. A Rh-coated pre-monochromator flat bent mirror was used for harmonic rejection and vertical collimation, while a bent cylindrical Rh-coated post-monochromator mirror was used for focusing. A Si(220) double crystal monochromator was used for energy selection. The samples were maintained below 10 K during data collection using an Oxford Instruments CF 1208 continuous-flow liquid helium cryostat. A Canberra solid-state Ge 100-element array detector was used to collect Kα fluorescence data.

Data reported here are up to k = 13.4 Å^{-1}. No noticeable interference from the Zn K-edge was observed. Internal energy calibration was performed by simultaneous measurement of the absorption of a copper foil placed between two ionization chambers located after the sample. The first inflection point of the foil spectrum was assigned to 8980.3 eV. Data were collected on two distinct and physically separate spots on the same sample to check for sample homogeneity. The data recorded here include an average of 6 scans with no change in the spectra between the scans.

XAS Data Analysis: The energy-calibrated averaged data were processed by fitting a second-order polynomial to the pre-edge region and subtracting this from the entire spectrum as a background. A three-region spline of orders 2, 3, and 3 was used to model the smoothly decaying post-edge region. The data were normalized by scaling the spline function to an edge jump of 1.0 at 9000 eV. This background subtraction and normalization was done using PySpline. The least-squares fitting program OPT in EXAFSPAK was used to fit the data. Initial *ab initio* theoretical phase and amplitude functions were generated in FEFF 7.0 using crystallographic parameters of bis((μ_2-iodo)-bis(3-cyanopyridine-N)-copper(I)) as the starting model. Atomic coordinates were adjusted as necessary as fits were improved. During the fitting process, the bond distance (R), and the mean-square thermal and static deviation in R (σ^2) were varied for all components. The threshold energy (E_0), the point at which the photoelectron wave vector k = 0 was chosen as 9000 eV, was also allowed to vary for each fit but was constrained to the same value for all components in a given fit. Coordination numbers (N) were systematically varied to provide the best chemically viable agreement to the EXAFS data and Fourier transform but was fixed within a given fit.

XAS Fit of [CuI(mCPy)]$_\infty$ (model A): The k^3-weighted Cu K-edge EXAFS data and Fourier transform (FT) of [CuI(mCPy)]$_\infty$ polymer are shown in Figure S15 and the EXAFS fit parameters are given in Table S. A first-shell Cu-N path at 2.05 Å is necessary to get a good fit to the data. A slight and not significant improvement in the fit is observed with a 1 Cu-N path rather than a 2 Cu-N path. The combination of 3 Cu-I and 2 Cu-Cu paths at 2.63 Å and 2.70 Å, respectively, gives the best fit to the second-shell (FT between 2 to 2.8 Å) data. The distance and σ^2 parameters for the two paths are

strongly correlated. A lower coordination number of 1 for the Cu-Cu path instead of 2 gives an equally good fit. Including only Cu-I or Cu-Cu paths gives an incomplete fit to the data. Other coordination numbers between 1-4 for Cu-Cu and Cu-I can be excluded based on a poorer fit factor, *F*, and/or higher σ^2. Fits to higher FT shells are not unique. The FT intensity between 3 to 3.5 Å (non-phase-shift corrected) can be fit with either 1 Cu-Cu path at ~3.6 Å or 1 Cu-I path at ~3.4 Å. The FT intensity between 3.5 to 4 Å (non-phase-shift corrected) can be fit with either 1 Cu-Cu at ~4.1 Å or two 1 Cu-I paths at ~3.8 Å and ~4.2 Å. The FT intensity between 4 and 5 Å (non-phase-shift corrected) can be fit with two 1 Cu-I or two 1 Cu-Cu paths or a combination of 1 Cu-I and 1 Cu-Cu paths. A 4 Cu-I-Cu path at 4.98 Å can also provide a good fit instead of Cu-I or Cu-Cu that has been used in the final fit.

Figures and Table

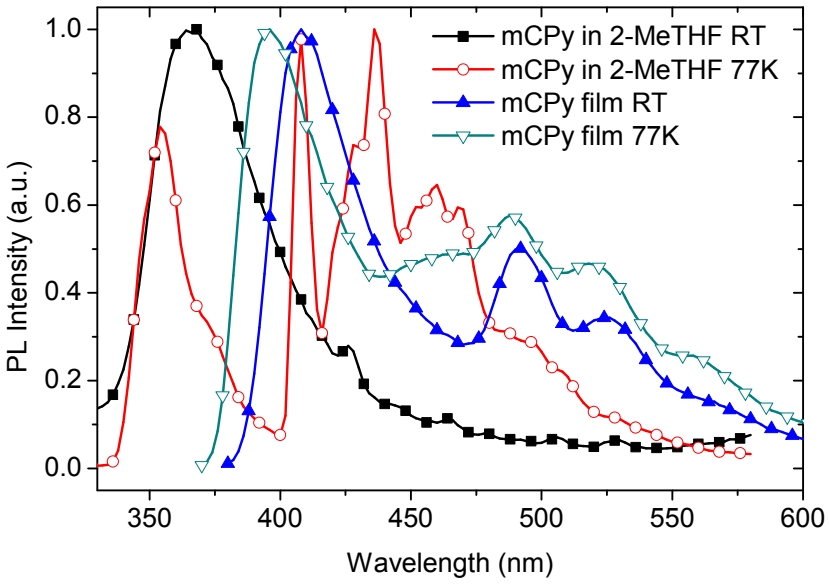

Figure S1 Photoluminescence spectra of mCPy film and mCPy in 2-MeTHF at 298 K and 77K with excitation wavelength of 300 nm.

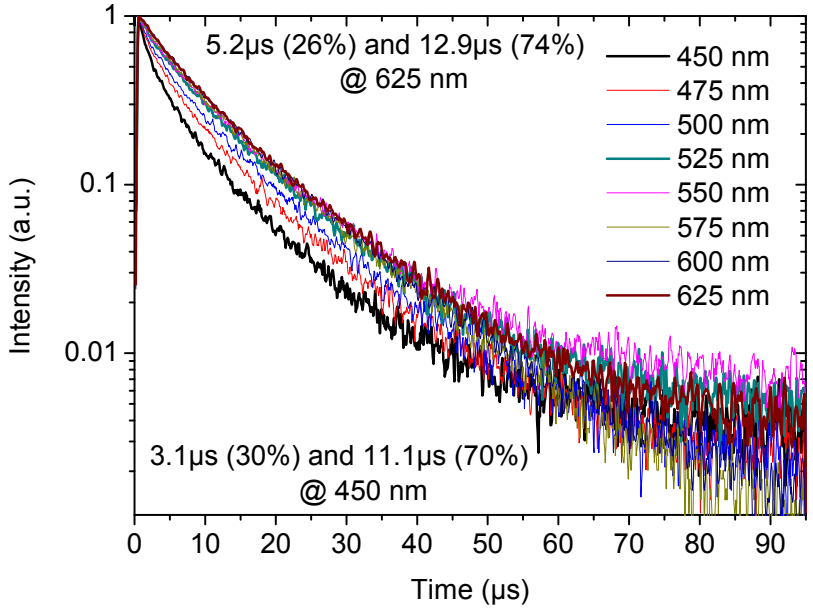

Figure S2 Decay lifetimes of codeposited CuI:mCPy (1:5) film measured at various wavelengths at room temperature with excitation energy of 331 nm.

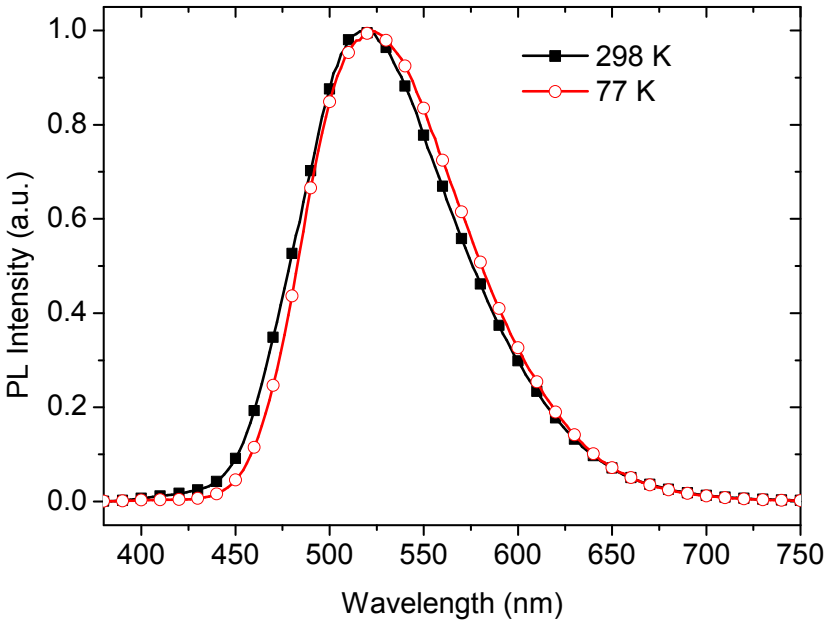

Figure S3 Photoluminescence spectra of codeposited CuI:mCPy (1:5) film at room temperature (298 K) and 77 K with excitation wavelength of 350 nm.

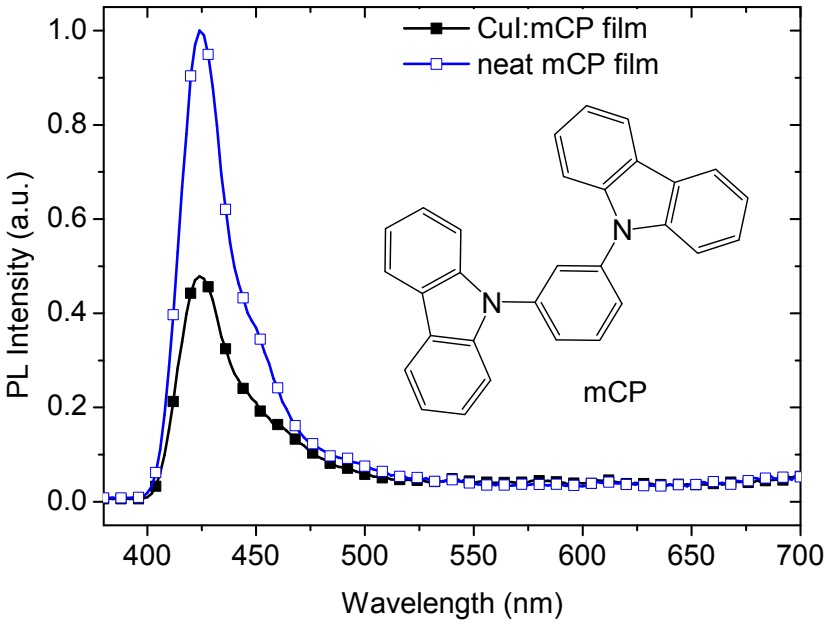

Figure S4 Photoluminescence spectra of mCP and CuI:mCP films at room temperature with excitation wavelength of 350 nm. Insert: chemical structure of mCP.

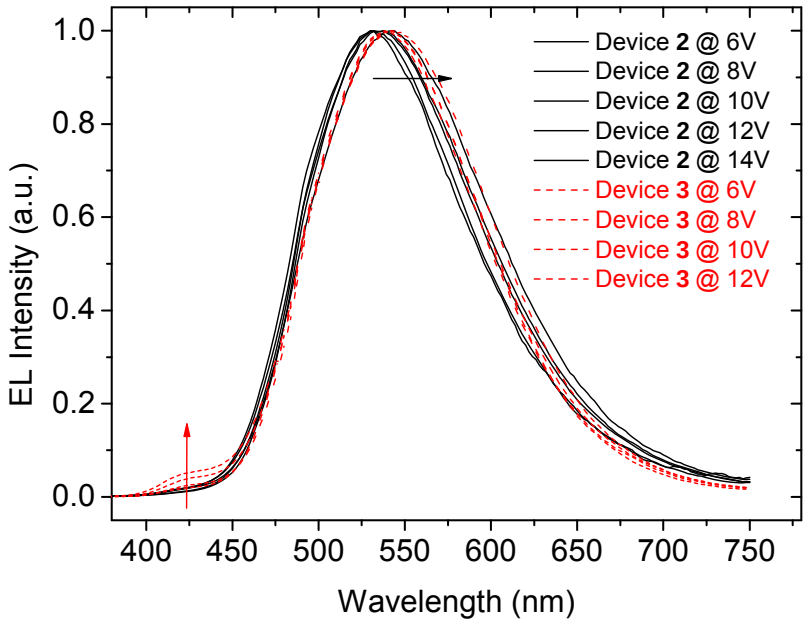

Figure S5 Electroluminescence spectra of devices **2** and **3** at different applied voltages.

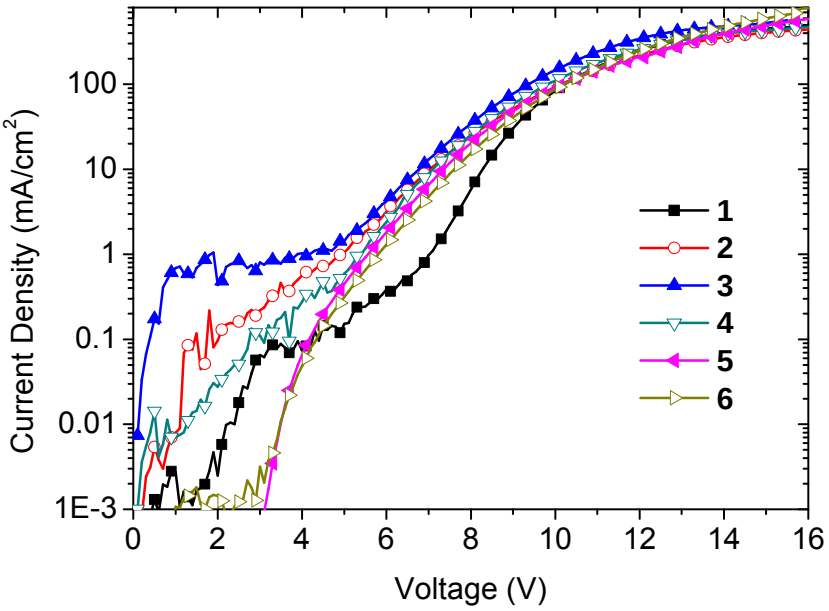

Figure S6 Current density-voltage curves of devices **1**-**6**.

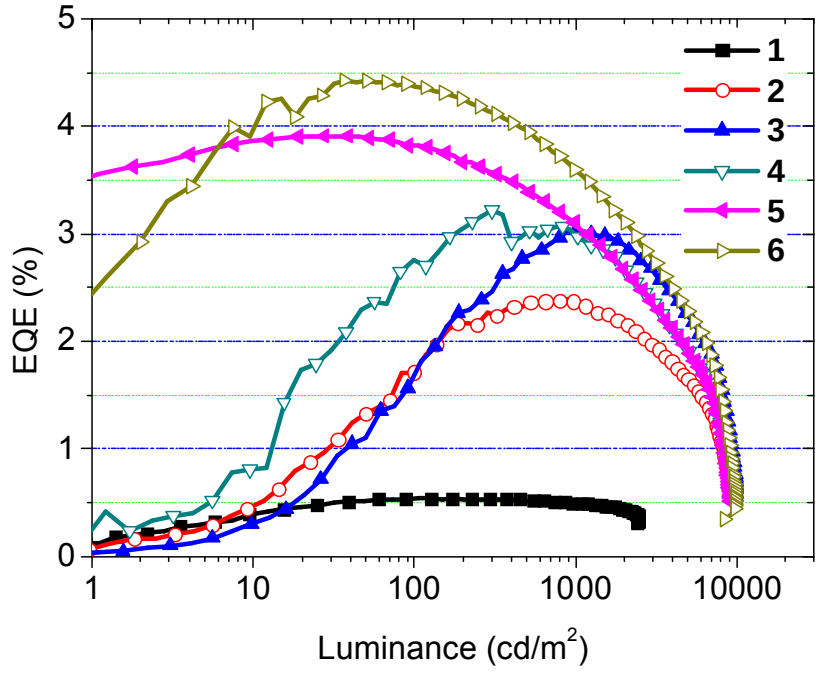

Figure S7 EQE-luminance curves of devices **1**-**6**.

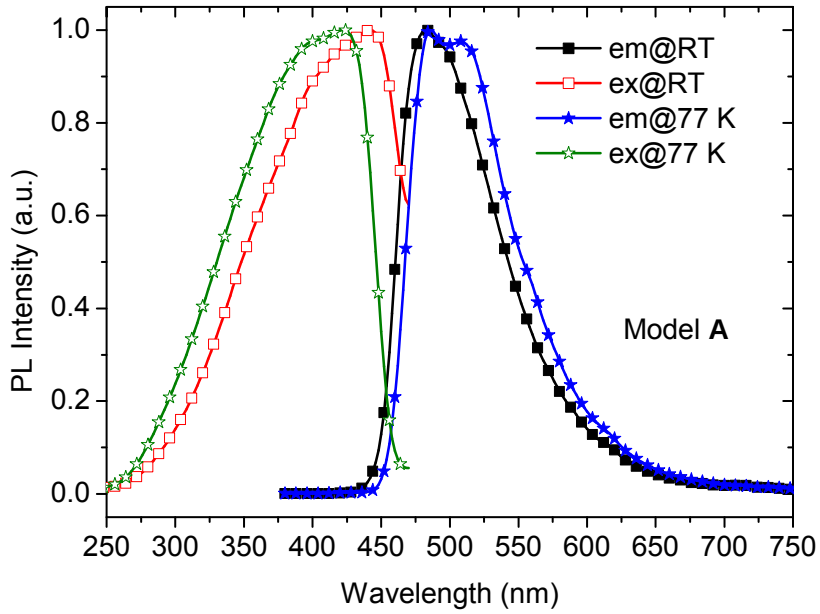

Figure S8 Photoluminescence and excitation spectra of $[CuI(mCPy)]_{\infty}$ (model **A**) at room temperature (RT, 298 K) and 77 K. The excitation and emission detection wavelengths were 350 and 480 nm, respectively.

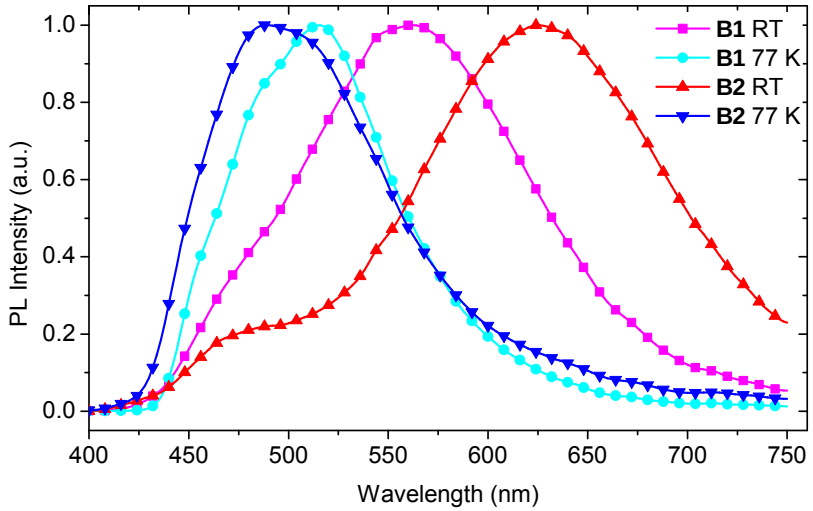

Figure S9 Photoluminescence spectra of $[CuI(mCPy)]_4 \cdot 3CH_2Cl_2$ (models **B1**) and $[CuI(mCPy)]_4$ (model **B2**) at room temperature (RT, 298 K) and 77 K with excitation wavelength of 380 nm.

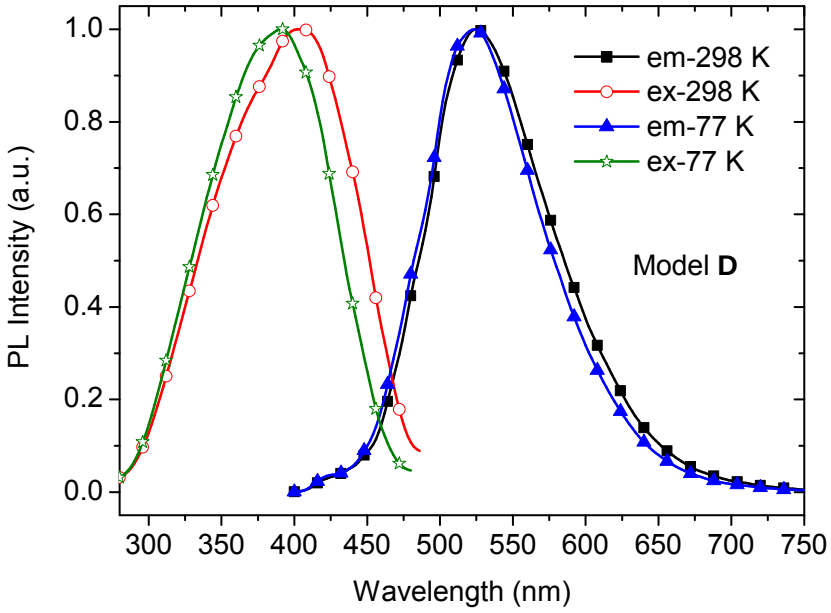

Figure S10 Photoluminescence and excitation spectra of codeposited CuI:mCPy powder sample (model **D**) at 298 K and 77 K. The excitation and emission detection wavelengths were 350 and 520 nm, respectively.

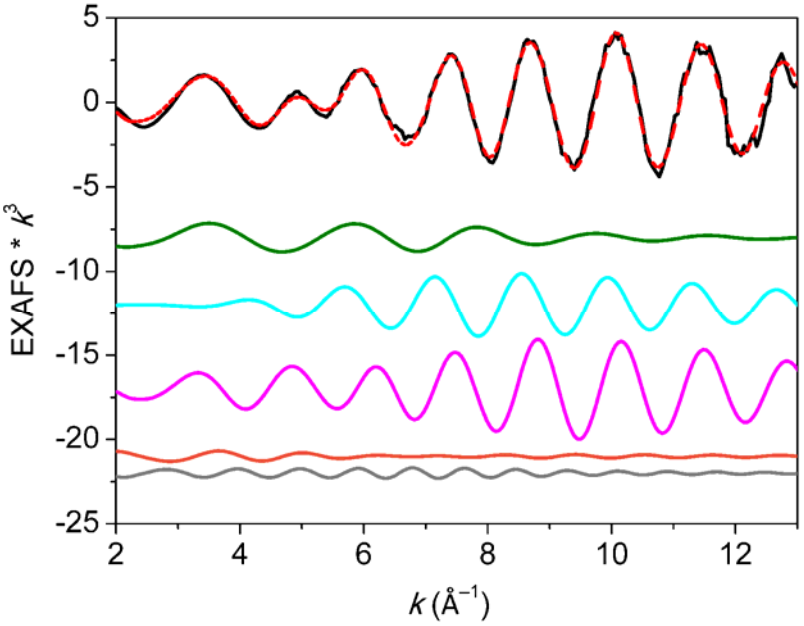

Figure S11 Cu K-edge EXAFS data to k = 13.4 Å^{-1} of CuI:mCPy codeposited film species (model **D**, CuI:mCPy = 1:2.5).

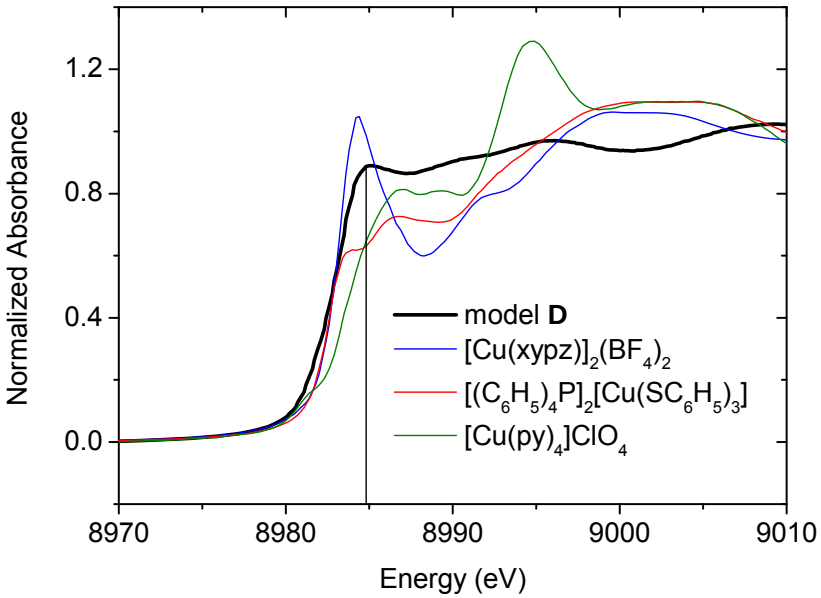

Figure S12 Cu K-edge of codeposited CuI:mCPy film species (model **D**), 2-coordinate Cu(I): $[Cu(xypz)]_2(BF_4)_2$, 3-coordinate Cu(I): $[(C_6H_5)_4P]_2[Cu(SC_6H_5)_3]$, and 4-coordinate Cu(I): $[Cu(py)_4]ClO_4$.

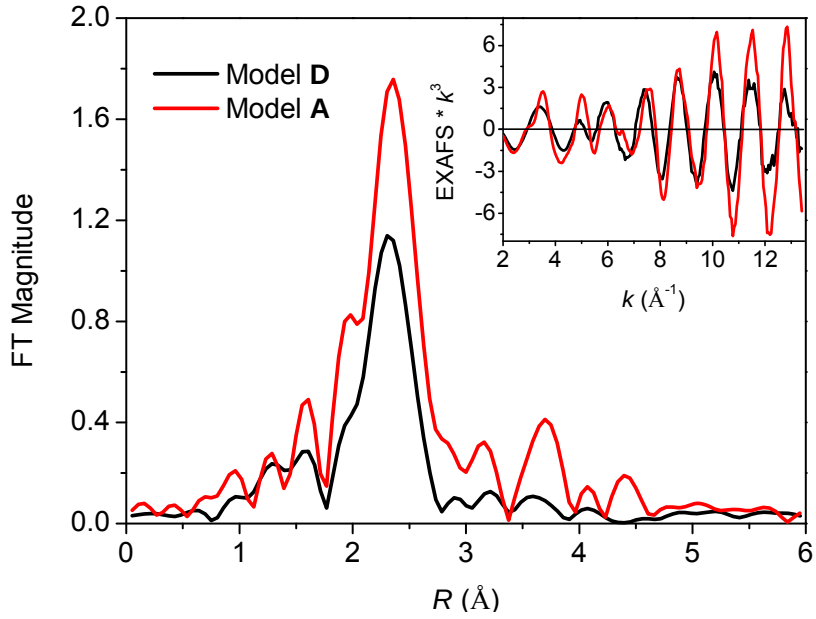

Figure S13 Cu K-edge EXAFS data to k = 13.4 $Å^{-1}$ (inset) and non-phase-shift-corrected Fourier transform of codeposited CuI:mCPy film species (model **D**), and $[CuI(mCPy)]_\infty$ polymer (model **A**). Phase shift in the first shell is ~0.4 Å.

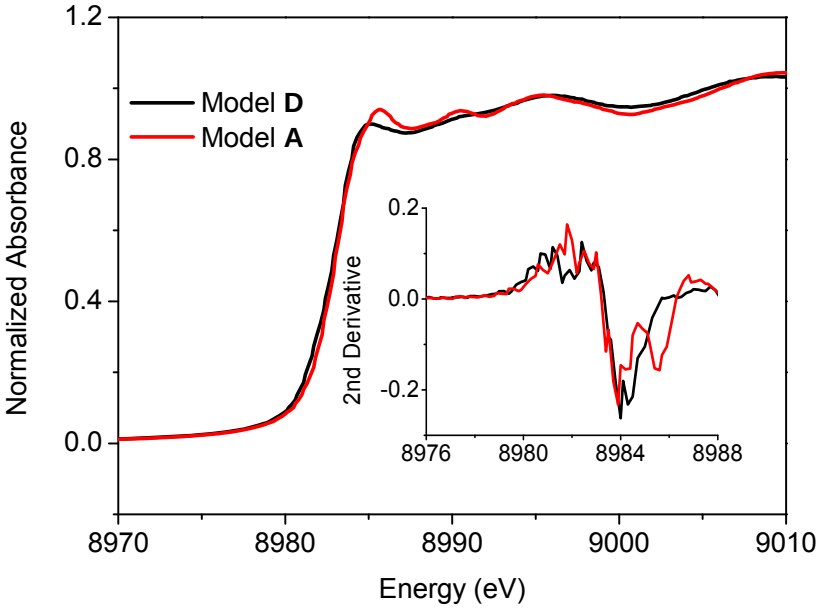

Figure S14 Cu K-edge of codeposited CuI:mCPy film species (model **D**) and $[CuI(mCPy)]_{\infty}$ polymer (model **A**). Inset shows the second derivative of the pre-edge.

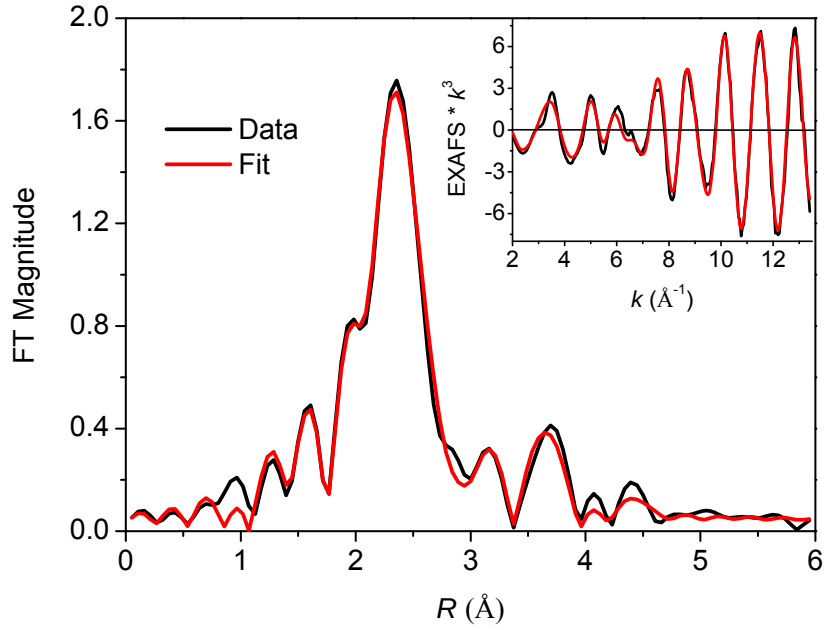

Figure S15. Cu K-edge EXAFS data to k = 13.4 Å^{-1} (inset) and non-phase-shift-corrected Fourier transform of $[CuI(mCPy)]_{\infty}$ (model **A**). Phase shift in the first shell is ~0.4 Å.

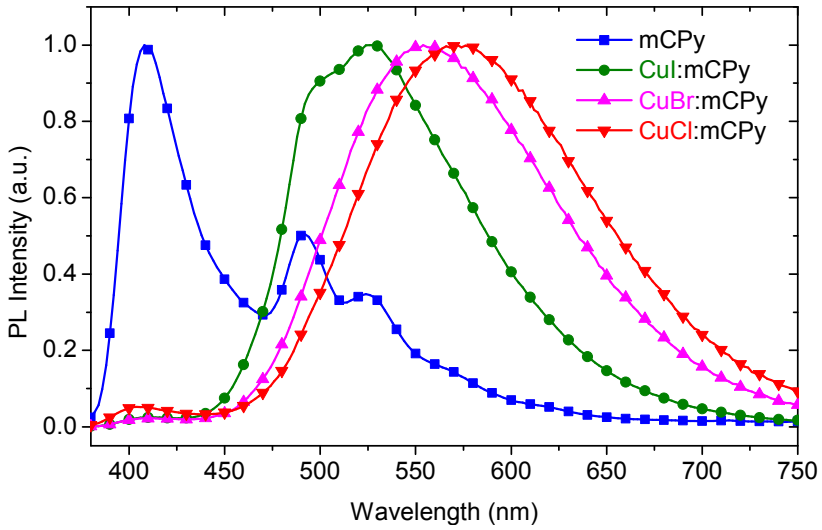

Figure S16 Photoluminescence spectra of mCPy, CuI:mCPy, CuBr:mCPy, and CuCl:mCPy films at room temperature with excitation wavelength of 350 nm.

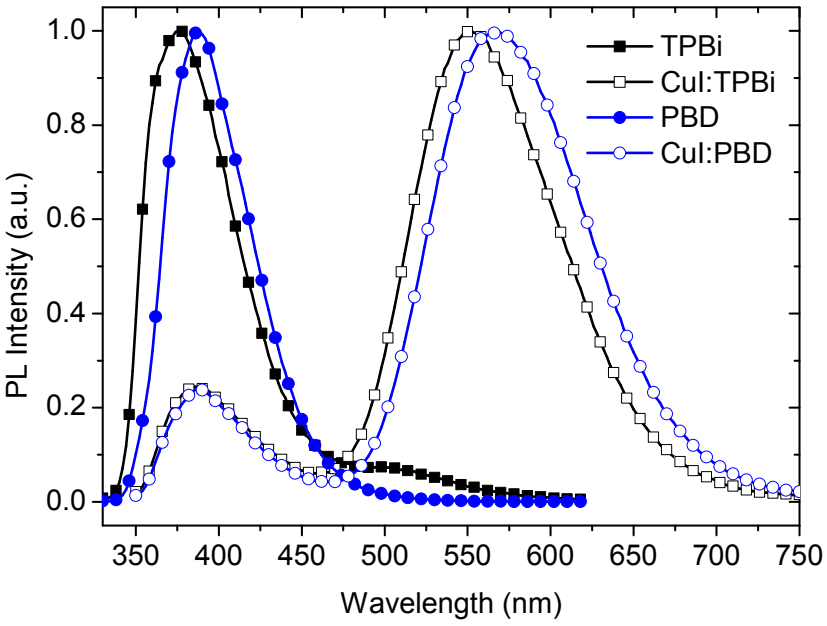

Figure S17 Photoluminescence spectra of TPBi, PBD, CuI:TPBi (1:4), and CuI:PBD (1:4) films at room temperature. The excitation wavelengths were 320 and 340 nm for neat films and codeposited films, respectively.

Table S1. EXAFS least-squares fitting results for k = 2–13.4 Å^{-1} for [CuI(mCPy)]$_\infty$ (model **A**)

Coord./Path	R(Å)[a]	σ^2(Å^2)[b]
1 Cu-N	2.05	223
3 Cu-I	2.63	476
2 Cu-Cu	2.70	863
1 Cu-Cu	3.64	671
1 Cu-I	3.85	574
1 Cu-I	4.23	946
4 Cu-I-Cu	4.98	561

F[c] = 0.227; ΔE_0(eV) = -12.13. [a]The estimated standard deviations in R for each fit is ±0.02 Å. [b]The σ^2 values are multiplied by 10^5. [c]The error, F, is given by $\Sigma[(\chi_{obsd} - \chi_{calcd})^2 k^6]/\Sigma[(\chi_{obsd})^2 k^6]$.